



Life modeling of a lithium ion cell with a spinel-based cathode

Long Cai ^a, Yiling Dai ^a, Marjorie Nicholson ^a, Ralph E. White ^{a,*}, Kamakshi Jagannathan ^b, Garima Bhatia ^b

^a Department of Chemical Engineering, University of South Carolina, Swearingen Engineering Center, 301 Main Street, Columbia, SC 29208, USA

^b India Science Lab, GMTCI, Bangalore 560066, India

HIGHLIGHTS

- A life model is developed by including the Mn dissolution for a lithium ion cell with spinel cathode.
- The radius change due the Mn dissolution is considered in the life model.
- The temperature effect on the Mn dissolution is included in the life model.
- The resistance of the inactive film generated due to the Mn dissolution is included in the life model.

ARTICLE INFO

Article history:

Received 25 May 2012

Received in revised form

14 August 2012

Accepted 16 August 2012

Available online 24 August 2012

Keywords:

Lithium ion battery

Life modeling

Moving boundary

Thermal effect

ABSTRACT

A life model is developed for a lithium ion cell with a spinel-based cathode. It is assumed in the proposed model that the Mn(III) disproportionation reaction causes the degradation of the spinel cathode. The Mn(III) disproportionation reaction leads to the Mn(II) dissolving into the electrolyte and the formation of an inactive material layer which causes a resistance increase in the cathode. The proposed model is used to investigate the effects of ambient temperature and voltage range of cycling on the loss of the cell capacity and the changes in the volume fraction of the cathode active material, the radius of the cathode particle and the resistance of the cathode.

© 2012 Elsevier B.V. All rights reserved.

1. Introduction

Spinel LiMn_2O_4 is of great interest as a cathode material for rechargeable lithium-ion batteries because of its low cost, high potential and safety. Especially, spinel LiMn_2O_4 maybe play great role in the near future for electric vehicle applications. However, this material exhibits serious capacity fading during cycling or storage at elevated temperature which makes it less competitive with other cathode materials.

Recent studies reveal that the capacity fading in spinel LiMn_2O_4 cathode is attributed to manganese dissolution [1,2]. There are at least two possible reasons for Mn dissolution: (1) Mn(II) dissolution into the electrolyte due to acid attack and a disproportion reaction of Mn(III) at the particle surface [3]; (2) the instability of the two-phase structure in the charged state which leads to the loss of MnO and the dissolution of Mn(II) to form a more stable single-phase structure [4]. In the cycle performance studies on the

spinel LiMn_2O_4 cathode, Jang et al. [5] and Xia et al. [4] found that manganese dissolution was notably high at the charged state (delithiated state) of the spinel LiMn_2O_4 cathode. Wang et al. [6] used rotating ring-disk collection experiments and found that the concentration of dissolved Mn(II) increases with cycle number and elevated temperature. In any cycle, the ring currents exhibited maxima corresponding to the end-of-charge (EOC) and end-of-discharge (EOD), while the largest peak occurred at the EOC state. The Mn dissolution from the spinel LiMn_2O_4 cathode occurs during cycling, especially in the charged state (i.e., the cathode potential is greater than 4.1 V) and in the discharged state (i.e., the cathode potential is less than 3.1 V).

The storage performance of a spinel LiMn_2O_4 cathode was also studied. Aoshima et al. [7] investigated the capacity loss of the spinel cathode at various states of charge (SOC) storage at 70 °C. The most significant capacity loss was observed in the case of the discharged cathode. Inoue and Sano [8] also found similar results. Their storage experiments at 80 °C with different additives revealed that water can accelerate the capacity fading of the spinel cathode.

Electrochemical impedance spectroscopy (EIS) studies revealed that the rate capacity loss due to the resistance increase is another

* Corresponding author. Tel.: +1 803 777 3270; fax: +1 803 777 0973.

E-mail address: white@cec.sc.edu (R.E. White).

important contribution due to spinel degradation [4,5,9–12]. The resistance increase in the spinel cathode resulted from: the SEI film building up due to the oxidation of electrolyte and the loss contact with the conducting additive due to the formation of inactive material in the Mn(III) disproportionation reaction.

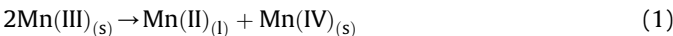
A mathematical model was developed by Park et al. [13] to simulate the degradation of spinel LiMn_2O_4 cathode based on the mechanism of Mn(III) disproportionation reaction by Lu and Lin [14]. Although the volume change in the active spinel cathode was taken into account, the change in the porosity of the spinel cathode due to the Mn dissolution was not included in their model.

A comprehensive pseudo two-dimensional (P2D) electrochemical thermal model for the degradation of the spinel LiMn_2O_4 cathode due to Mn(III) disproportionation reaction is developed in this paper. The proposed model includes the volume changes in both the active material and the inactive material in the cathode, the radius change in the cathode solid particles, the porosity change in the cathode, and film resistance increase in the cathode due to Mn(III) disproportionation reaction. The proposed model was applied to simulate the cycling performance at different temperatures and voltage ranges for a lithium-ion cell which consists of a spinel LiMn_2O_4 cathode, Celgard's 25 μm (in thickness) separator, a carbon-based anode and 1 M LiFP_6 in PC/EC/DMC (1:1:1 volume ratio) electrolyte.

2. Model development

2.1. Modeling of Mn dissolution

It is assumed that the Mn dissolution occurs according to the following disproportionation reaction of Mn(III) [5,13,14]:



where $\text{Mn(III)}_{(\text{s})}$ is the active Mn with the valence of 3 in the spinel cathode, $\text{Mn(II)}_{(\text{l})}$ is the product in the disproportionation reaction with the valence of 2 and is soluble in the electrolyte, and $\text{Mn(IV)}_{(\text{s})}$ is another product with the valence of 4 and remains in the solid phase but is inactive for the Li^+ insertion/deintercalation reaction. The disproportionation reaction of Mn(III) is not an electrochemical reaction and occurs all the time (except for a fully charged cell where all Mn is Mn(IV)) as long as the cell is assembled. The reaction rate of the disproportionation reaction depends on the temperature only. It was proposed that the conversion of reaction (1) is a function of time and is given by [14]:

$$1 - (1 - X_a)^{1/3} = kt \quad (2)$$

where k is the reaction rate constant (1/s), and X_a is the conversion of the dissolution reaction shown in Eq. (1) and is defined by:

$$X_a = \frac{(\text{Number of moles of the dissolved Mn(II) in the electrolyte}) \times 2}{\text{Number of moles of the Mn(III) in the spinel cathode}} \quad (3)$$

The reaction rate constant is defined by:

$$k = k_0 \exp\left(-\frac{E_{ar}}{RT}\right) \quad (4)$$

where k_0 is the pre-exponential coefficient, s^{-1} , and E_{ar} is the activation energy related to k .

The cathode active material, LiMn_2O_4 , can be rewritten as $\text{LiMn(III)Mn(IV)O}_4$, where Mn(III) is the active part which reacts with Li in the electrochemical reaction. Rewrite Eq. (1) in terms of the active material and the products with the same number of Mn atoms in the dissolution reaction as:



where A denotes the active material (LiMn_2O_4) which is consumed due to the dissolution reaction, S is the solid phase product with two Mn atoms in 4 valence (Mn(IV)_2) and L is the liquid phase product with two Mn atoms in 2 valence (Mn(II)_2). Because A, S and L consist of two Mn atoms, it is assumed that A, S and L have approximately the same molar volumes. We denote the remaining active material (LiMn_2O_4) as R. Thus, the sum of volumes of A and R is a constant which is the initial volume of the active material: V_0 , that is:

$$V_0 = V_R + V_A \quad (6)$$

where V_R and V_A denote the volumes of R and A, respectively. According to the stoichiometry in Eq. (5) and along with the assumption that the molar volumes of A, S and L are the same, we have the following relationships:

$$V_L = \frac{1}{4}V_A \quad (7)$$

$$V_S = \frac{3}{4}V_A \quad (8)$$

Eq. (3) can be rewritten as:

$$X_a = \frac{(2 \text{ moles L}) \times 2}{1 \text{ mole R}} = \frac{4 \text{ mole L}}{1 \text{ mole R}} \quad (9)$$

Since we assumed that the molar volumes of L and R are the same, Eq. (9) is equivalent to the following equation:

$$X_a = \frac{4V_L}{V_R} \quad (10)$$

Substitution of Eq. (7) into Eq. (10) yields:

$$X_a = \frac{V_A}{V_R} \quad (11)$$

Eq. (11) indicates that the conversion of Mn dissolution reaction equals the volume of the dissolved active material divided by the volume of the remaining active material.

The initial volume fraction of the active material in the spinel cathode is defined by:

$$\varepsilon_{v,p}^0 = \frac{V_0}{V_{\text{cath}}} \quad (12)$$

where V_{cath} is the volume of the cathode. The volume fraction of the remaining active material is given by:

$$\varepsilon_{v,p} = \frac{V_R}{V_{\text{cath}}} \quad (13)$$

By substituting Eqs. (7), (8), (11) and (12) into Eq. (13), we have:

$$\varepsilon_{v,p} = \varepsilon_{v,p}^0 \frac{1}{1 + X_a} \quad (14)$$

The volume fraction of the inactive material, $\varepsilon_{iv,p}$, in the solid phase is defined by:

$$\varepsilon_{iv,p} = \frac{V_S}{V_{\text{cath}}} = \varepsilon_{v,p}^0 \frac{\frac{3}{4} V_A}{V_0} = \frac{3}{4} \varepsilon_{v,p}^0 \frac{X_a}{1 + X_a} \quad (15)$$

The porosity of the cathode, ε_p , is determined by:

$$\varepsilon_p = 1 - \varepsilon_{v,p} - \varepsilon_{iv,p} - \varepsilon_{f,p} \quad (16)$$

where $\varepsilon_{f,p}$ is the volume fraction of the filler in the cathode. By substituting Eqs. (14) and (15) into Eq. (16), we have:

$$\varepsilon_p = 1 - \varepsilon_{v,p}^0 \frac{1 + 0.75X_a}{1 + X_a} - \varepsilon_{f,p} \quad (17)$$

The radius of the active material in the cathode solid particle and the radius of the solid particle are illustrated in Fig. 1.

The volume of the remaining active material as a function of the initial volume of the solid particle is obtained by substituting Eq. (11) into Eq. (6):

$$V_R = \frac{V_0}{(1 + X_a)} \quad (18)$$

The volume of the solid phase as a function of time is given by:

$$V(t) = V_S + V_R \quad (19)$$

Substitution of Eqs. (7), (11) and (18) into Eq. (19) yields:

$$V(t) = \frac{1 + 0.75X_a}{1 + X_a} V_0 \quad (20)$$

According to Eq. (18), the relationship between the radius of the active particle and the initial radius of the particle is given by:

$$R_{a,p}(t) = \left(\frac{1}{1 + X_a} \right)^{1/3} R_p \quad (21)$$

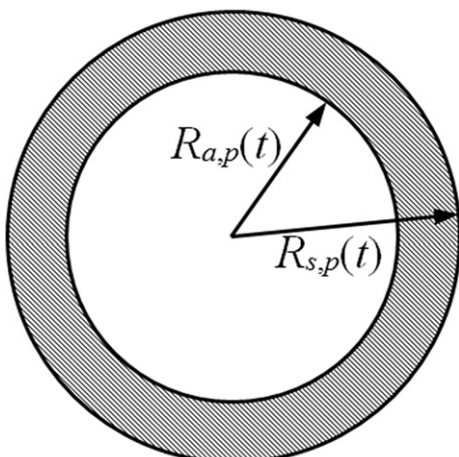


Fig. 1. Radius change in a solid particle due to Mn dissolution.

where R_p is the initial radius of the particle and $V_0 = 4/3\pi R_p^3$. Based on Eq. (20), the radius of the solid particle, $R_{s,p}(t)$, as a function of time is given by:

$$R_{s,p}(t) = \left(\frac{1 + 0.75X_a}{1 + X_a} \right)^{1/3} R_p \quad (22)$$

Since the inactive solid phase grows as the dissolution reaction occurs, the resistance of this inactive material layer increases. Consequently, we introduce a variable, R_{film} , to denote the film resistance in the cathode particle. We also assume that this film resistance depends on X_a as follows:

$$R_{\text{film}} = R_{\text{film}}^0 + R_{\text{SEI}} \frac{R_{s,p}(t) - R_{a,p}(t)}{R_p} \quad (23)$$

where R_{film}^0 is the initial film resistance and R_{SEI} is the resistance of the inactive material.

2.2. Electrochemical model

A schematic of a typical Li-ion cell consisting of three regions namely a positive electrode (spinel LiMn_2O_4), a separator (polypropylene), and a negative electrode (carbon-based) is shown in Fig. 2. A physics-based pseudo two-dimensional (P2D) electrochemical model which developed by Newman et al. [15] was applied to simulate a lithium ion cell with a spinel cathode and a carbon-based anode as shown in Fig. 2. The P2D electrochemical model consists of the material balance in the solid particles in the micro scale (r -direction in Fig. 2), the material balance in the binary electrolyte which fills the pores in the porous electrodes and the separator, and the charge balances in the solid matrix in the electrodes and in the electrolyte. The governing equations of the P2D model are summarized in Appendix A besides of the material balance of Li^+ in the solid particles in the cathode. The open circuit potentials of the spinel cathode and the carbon-based anode and other model expressions are summarized in Appendix B.

The simulation of lithium ions diffusion in the cathode material with multi-phases in a lithium ion cell has been widely investigated by using the sharp interface models (i.e., the shrinking core model [16] and the moving boundary model [17]) and the phase field model [18] which is a non-Fickian behavior and interfaces tracking free model. We assumed that the Mn dissolution reaction (Reaction (1)) only occurs on the interface between the active spinel and the

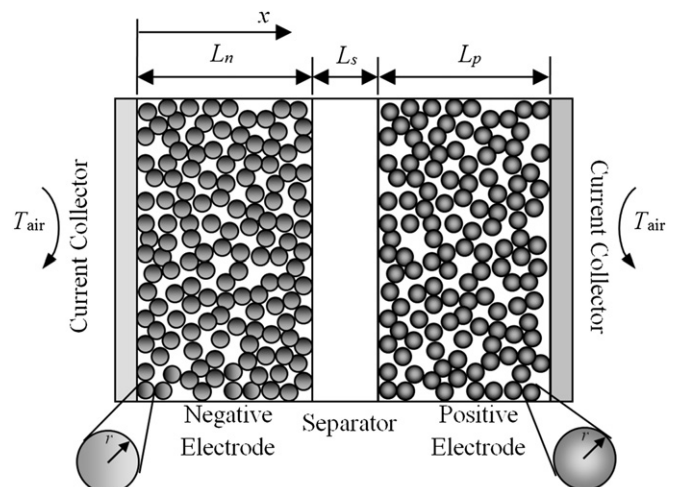


Fig. 2. Schematic of a Li-ion cell.

electrolyte. This produces an inactive solid porous layer (shown in Fig. 1) on the surface of the particle. Consequently, the electrolyte can penetrate the inactive porous layer and reach the surface of the active spinel where the Li insertion/extraction reaction occurs. Based on these assumptions a moving boundary model is applied to simulate the diffusion of Li ions in the active spinel. The material balance of Li^+ in the solid particles in the cathode with a moving reaction boundary which is shown in Fig. 1 is given by:

$$\frac{\partial c_{s,p}}{\partial t} = \frac{1}{r^2} \frac{\partial}{\partial r} \left(D_{s,p} r^2 \frac{\partial c_{s,p}}{\partial r} \right) \quad (24)$$

with the boundary conditions:

$$-D_{s,p} \frac{\partial c_{s,p}}{\partial r} \Big|_{r=0} = 0 \quad (25)$$

$$-D_{s,p} \frac{\partial c_{s,p}}{\partial r} \Big|_{r=R_{a,p}(t)} = j_p \quad (26)$$

and the initial condition:

$$c_{s,p}(t=0) = c_{s,p,0} \quad (27)$$

where $D_{s,p}$ is the diffusion coefficient of Li^+ in the solid particles in the cathode, j_p is the pore wall flux in the cathode, and $c_{s,p,0}$ is the initial concentration of Li^+ in the particles.

Since the radius of the active part of the cathode, $R_{a,p}$, is varying with time, it is more convenient to convert Eqs. (24)–(27) into the dimensionless spatial coordinate, y , which is defined by:

$$y = \frac{r}{R_{a,p}} \quad (28)$$

Eqs. (24)–(26) in the dimensionless spatial coordinate, y , with fixed boundaries are given by:

$$\begin{aligned} \frac{\partial c_{s,p}}{\partial t} &= \frac{1}{R_{a,p}^2 y^2} \frac{\partial}{\partial y} \left(D_{s,p} y^2 \frac{\partial c_{s,p}}{\partial y} \right) \\ -D_{s,p} \frac{\partial c_{s,p}}{\partial y} \Big|_{y=0} &= 0 \\ -D_{s,p} \frac{\partial c_{s,p}}{\partial y} \Big|_{y=1} &= R_{a,p} j_p \end{aligned} \quad (29)$$

2.3. Thermal model

The energy balance for the cell is given by [19]:

$$\rho_i C_{p,i} \frac{dT_i}{dt} = \frac{\partial}{\partial x} \left(\lambda_i \frac{\partial T_i}{\partial x} \right) + Q_{rxn,i} + Q_{rev,i} + Q_{ohm,i} \quad (30)$$

where ρ_i is the density of cell component i ($i = p$ for the cathode, $i = s$ for the separator, and $i = n$ for the anode), $C_{p,i}$ is the specific heat of the component i , λ_i is the thermal conductivity of component i , $Q_{rxn,i}$ is the heat generation rate due to electrochemical reaction in electrode i , $Q_{rev,i}$ is the heat generation rate due to reversible reaction in electrode i , and $Q_{ohm,i}$ is the heat generation rate due to Ohmic loss in component i . The three types of heat generation rates are defined as follows:

$$Q_{rxn,i} = F a_i j_i (\phi_{1,i} - \phi_{2,i} - U_i), \quad i = p, n \quad (31)$$

where U_i is the open circuit potential of electrode i .

$$Q_{rev,i} = F a_i j_i T_i \left[\frac{\partial U}{\partial T} \right]_i \quad (32)$$

where $[\partial U / \partial T]_i$ is the open circuit potential change rate due to the change in temperature in electrode i evaluated at the reference temperature T_{ref} . The expressions of $[\partial U / \partial T]_i$ as functions of state of charge for the electrodes are presented in Appendix B.

$$\begin{aligned} Q_{ohm,i} &= \sigma_{eff,i} \left(\frac{\partial \phi_{1,i}}{\partial x} \right)^2 + \kappa_{eff,i} \left(\frac{\partial \phi_{2,i}}{\partial x} \right)^2 + \frac{2\kappa_{eff,i} R T_i}{F} (1 - t_+^0) \\ \frac{1}{c_i} \frac{\partial c_i}{\partial x} \frac{\partial \phi_{2,i}}{\partial x}, \quad i &= p, n \end{aligned} \quad (33)$$

and

$$Q_{ohm,s} = \kappa_{eff,s} \left(\frac{\partial \phi_{2,s}}{\partial x} \right)^2 + \frac{2\kappa_{eff,s} R T_s}{F} (1 - t_+^0) \frac{1}{c_s} \frac{\partial c_s}{\partial x} \frac{\partial \phi_{2,s}}{\partial x} \quad (34)$$

The initial condition for the temperature is given by the ambient temperature:

$$T(t=0) = T_{air} \quad (35)$$

where T_{air} is the ambient temperature. The boundary conditions are determined by Newton's cooling law:

$$-\lambda_n \frac{\partial T}{\partial x} \Big|_{x=0} = h_{coef} (T_{air} - T) \quad (36)$$

$$-\lambda_p \frac{\partial T}{\partial x} \Big|_{x=L_p+L_s+L_n} = h_{coef} (T - T_{air}) \quad (37)$$

where h_{coef} is the heat transfer coefficient.

Table 1 shows the values of the model parameters.

Table 1
Model parameters.

Parameter	Value	Parameter	Value
L_p	135e-6 m	σ_p^a	3.8 S m ⁻¹
L_s	25e-6 m	σ_n^a	100 S m ⁻¹
L_n	100e-6 m	$D_{s,p,ref}^a$	1.0e-13 m ² s ⁻¹
R_p^a	8e-6 m	$D_{s,n,ref}^a$	3.9e-14 m ² s ⁻¹
R_n^a	12.5e-6 m	$k_{p,ref}^b$	2.0e-10 mol ^{0.5} m ^{2.5} s ⁻¹
ε_p^a	0.444	$k_{n,ref}^b$	2.0e-10 mol ^{0.5} m ^{2.5} s ⁻¹
ε_s^b	0.41	k_0^c	3.41e5 s ⁻¹
ε_n^a	0.357	E_{ar}^c	72.48e3 J mol ⁻¹
$\varepsilon_{f,p}^b$	0.252	$E_{ad,p}^b$	2.9e3 J mol ⁻¹
$\varepsilon_{f,n}^b$	0.172	$E_{ad,n}^b$	3.5e3 J mol ⁻¹
$\varepsilon_{f,p}^0$	$1 - \varepsilon_p - \varepsilon_{f,p}$	$E_{ak,p}^b$	5.8e3 J mol ⁻¹
$\varepsilon_{f,n}^0$	$1 - \varepsilon_n - \varepsilon_{f,n}$	$E_{ak,n}^b$	2.0e3 J mol ⁻¹
$\varepsilon_{h,p}^0$	0	λ_p^d	1.58 W m ⁻¹ K ⁻¹
R	8.314 J mol ⁻¹ K ⁻¹	λ_s^d	0.344 W m ⁻¹ K ⁻¹
F	964.87 C equiv ⁻¹	λ_n^d	1.04 W m ⁻¹ K ⁻¹
T_{ref}	298.15 K	ρ_p^d	2328.5 kg m ⁻³
T_{air}	328.15 K	ρ_s^d	1008.98 kg m ⁻³
t_+^0	0.363	ρ_n^d	1347.33 kg m ⁻³
$brugg_p^b$	1.5	$C_{p,p}^d$	1269.21 J kg ⁻¹ K ⁻¹
$brugg_s^b$	1.5	$C_{p,s}^d$	1978.16 J kg ⁻¹ K ⁻¹
$brugg_n^b$	1.5	$C_{p,n}^d$	1437.4 J kg ⁻¹ K ⁻¹
I_{app}	35 A m ⁻²	$\alpha_{a,p}$	0.5
$C_{s,p,max}^a$	228.60 mol m ⁻³	$\alpha_{c,p}$	0.5
$C_{s,n,max}^a$	263.90 mol m ⁻³	$\alpha_{a,n}$	0.5
$\theta_{p,0}^b$	0.30	$\alpha_{c,n}$	0.5
$\theta_{n,0}^b$	0.75	R_{film}^b	1.0e-3 Ω m ²
c_0^a	2000 mol m ⁻³	h_{coef}	2.0 W m ⁻² K ⁻¹

^a Obtained from Ref. [20].

^b Assumed.

^c Obtained from Ref. [14].

^d Obtained from COMSOL model library.

3. Results and discussion

The IDA package, which can be used to solve initial value problems for differential/algebraic equation systems, in SUNDIALS (Suite of Nonlinear and Differential/Algebraic Equation Solvers) [21] was applied to solve the P2D thermal model associated with the proposed Mn dissolution model. The finite volume method (FVM) was applied to discretize the spatial coordinates. By using FVM, the cathode and anode were portioned into 50 finite volumes and the separator and the particles in *r*-direction (shown in Fig. 2) are divided into 25 finite volumes. The SI unit system was applied in the system. The relative and the absolute tolerances were selected as 1.0e-9 for all of the dependent variables in the system. The in-house C code was validated by comparing the results obtained from the in-house C code to those obtained from COMSOL [22] in which the same equations were solved and the same tolerances were used.

Four case studies were carried out using our in-house C code. The cell mentioned in the previous section was discharged and charged fifty times at constant current rate of 2C (1C = 17.5 A m⁻²) with two different ambient temperatures: 25 °C and 55 °C and two different voltage ranges: [3.2, 4.0] V and [3.5, 4.3] V.

Fig. 3 shows the normalized capacity obtained during the 2C discharge vs. the cycle number for the four cases. The normalized capacity in the *i*th cycle, $N\text{Cap}_i$, is obtained as follows:

$$N\text{Cap}_i = \frac{\text{Cap}_i}{\text{Cap}_1} \quad (38)$$

where $N\text{Cap}_i$ is the normalized discharge capacity in cycle *i*, Cap_i is the discharge capacity in cycle *i* and Cap_1 is the discharge capacity in cycle 1. Fig. 3 indicates that the cell capacity loss is more significant due to the spinel cathode degradation when the cell is cycled at a higher ambient temperature within the same voltage range. It is also found from Fig. 3 that at the same ambient temperature, the cell cycled in a higher voltage range (i.e., 3.5–4.3 V) loses more capacity. As mentioned in the previous section, we assumed that the Mn dissolution reaction does not depend on the state of charge of the spinel cathode. The difference in the voltage range only affects the discharge time and the cell temperature which cause the difference in the degradation rate of the spinel cathode. The discharge time for a cell discharged at 2C in the voltage range of 3.5–4.3 V is longer than that for a cell discharged at 2C in the voltage range of 3.2–4.0 V.

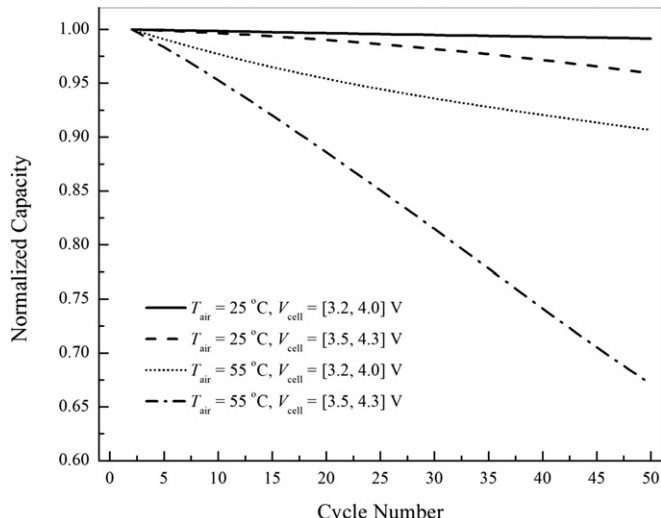


Fig. 3. Normalized discharge capacity vs. cycle number.

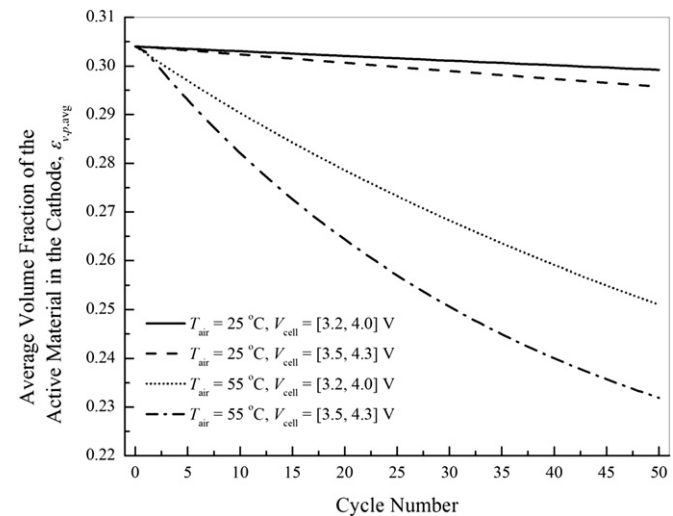


Fig. 4. Averaged volume fraction of the active cathode at the end of discharge vs. the cycle number.

Also the cell temperature is a slightly higher in the cell cycled within 3.5–4.3 V than in the cell cycled within 3.2–4.0 V. The capacity loss shown in Fig. 3 is the combination of the contributions of the loss of the active spinel cathode due to Mn dissolution reaction and the resistance increase on the spinel cathode.

Fig. 4 shows the change in the average volume fraction of the active material in the spinel cathode with cycle number in the four case studies. Initially, the volume fraction of the active material in the spinel cathode is 0.304. The average volume fraction of the active spinel cathode decreases with the cycle number due to the Mn dissolution reaction. Fig. 4 shows that the degradation rate of the active spinel cathode is slow for the cell cycled at the ambient temperature of 25 °C, but the degradation of the cathode is enhanced significantly when the ambient temperature is as high as 55 °C. Fig. 4 also indicates that for the same ambient temperature, the cell loses more active material when it is cycled within the voltage range 3.5–4.3 V than the cell cycled within the voltage range 3.2–4.0 V due to the difference in the operating time. The

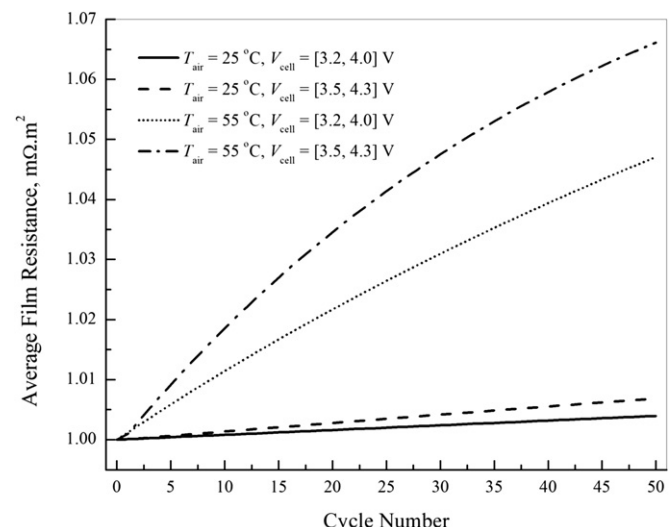


Fig. 5. Averaged film resistance at the end of discharge vs. cycle number.

theoretical capacity remaining in the spinel cathode in the cell cycled with $T_{\text{air}} = 55^\circ\text{C}$ and voltage range 3.5–4.3 V is about 76.28%.

The average film resistance varying with cycle number is presented in Fig. 5 for the four cases. The Mn dissolution reaction which is shown in Eq. (1) not only causes the loss of active spinel cathode but also causes the increase in the film resistance on the spinel cathode. As the Mn dissolution reaction proceeds during cycling of the cell, the thickness of the inactive layer, which is shown in Fig. 1 and assumed electronically conductive, is growing. As a result of the growing inactive film, the film resistance increases accordingly. The temperature and voltage range effects on the film resistance is similar but in the opposite direction (increasing film resistance while the volume fraction of the active cathode decreases) as on the loss of the active spinel cathode volume fraction.

Fig. 6 shows the cell voltages during the 2C discharge within 3.5–4.3 V and at the ambient temperature of 55 °C in the first cycle and the last (50th) cycle. The discharge capacity remaining is about 67% for the cell cycled under the condition: $T_{\text{air}} = 55^\circ\text{C}$ and voltage range 3.5–4.3 V, while the remaining theoretical capacity in the cell is about 76.28% as shown in Fig. 4. The difference between the available capacity and the theoretical capacity is due to the difference in the cell resistance. Fig. 6 shows that the potential drop from the end of charge (4.3 V) to the beginning of a 2C discharge increases about 1.5 times in the 50th cycle compared to the first cycle.

Fig. 7 shows the normalized radius change with the cycle number. The radii of the active material ($R_{\text{a,p}}$) and the solid particle ($R_{\text{s,p}}$) are normalized by dividing by the original radius of the particle (R_p) in the spinel cathode. The four shadows in Fig. 7, each of which is enclosed by two thick lines (top line denotes the normalized radius of the solid particle and the bottom line denotes the normalized radius of the active cathode part), are obtained from the four case studies. In each case, the difference between the radius of the solid particle and the radius of the active cathode part indicates the thickness of the inactive film. The change in the radius of the active part in the spinel cathode is consistent to the change in the volume fraction of the active material which is shown in Fig. 4. Eqs. (18) and (20) indicate that as time goes infinity, the conversion of the Mn dissolution reaction is infinity, as a result, the volume of the active part is vanished and the volume of the remaining inactive

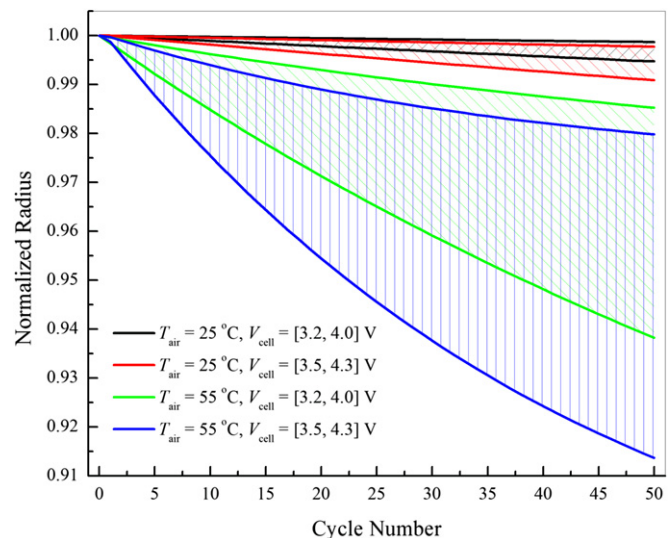


Fig. 7. Radius change with the cycle number.

solid is 3/4 of the initial volume of the active cathode. Consequently, as time goes to infinity $R_{\text{a,p}}$ is zero and $R_{\text{s,p}} = \sqrt[3]{0.75}R_p$ which are indicated in Eqs. (21) and (22), respectively.

The mechanism of Mn dissolution mentioned in Eqs. (2)–(4) only considers the chemical reaction effects. The parameter values for k_0 and E_{ar} used in Eq. (4) were obtained from the experiments, [14] which consisted of immersing LiMn_2O_4 in the electrolyte at different temperatures. It has been reported that the Mn dissolution rate also depends on the state of charge, [6] the composition of the spinel electrode, [23] the type of solute in the electrolyte, [24] etc. Our future work will be to develop a modified mechanism of Mn dissolution by including an electrochemical reaction effect.

4. Conclusion

A mathematical model for Mn dissolution in a lithium ion cell with a spinel-based cathode was developed and was applied in an electrochemical thermal model to predict the cathode degradation during a constant current charge/discharge cycling process under two selected ambient temperatures of 25 and 55 °C and within two selected voltage ranges of 3.2–4.0 V and 3.5–4.3 V. It was assumed in the proposed model that the cathode degradation is due to the Mn(III) disproportionation reaction: $2\text{Mn(III)}_{(\text{s})} \rightarrow \text{Mn(II)}_{(\text{l})} + \text{Mn(IV)}_{(\text{s})}$. As a result, the Mn^{2+} ions dissolve in the electrolyte which may transfer to the anode and deposit on the anode to lead to anode degradation. On the other hand, Mn(IV) which is inactive remains in the solid phase and causes an increase in the cathode resistance. The proposed model includes the effects of change in the radius of the cathode active material particles, change in the cathode porosity and change in the film resistance on the cathode degradation. The case studies reveal that the cathode loses its active material as the ambient temperature increases and the voltage range goes higher where the cell operational time is higher. The case studies also indicate that the ambient temperature plays the most important role in the Mn dissolution reaction.

Acknowledgment

This work was funded by General Motors Global R&D, India Science Lab.

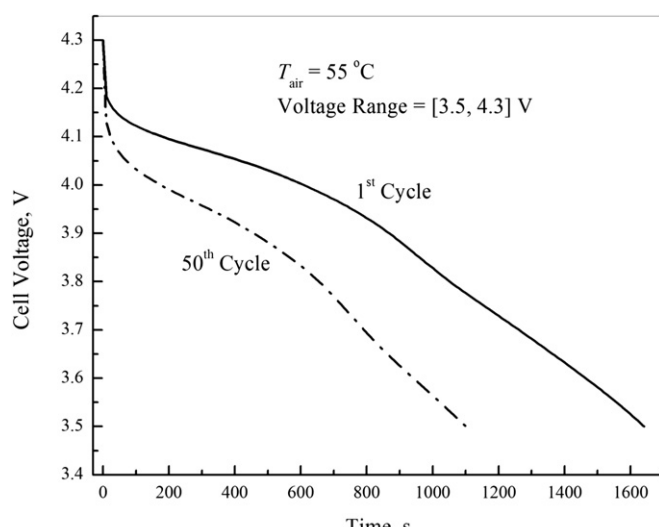


Fig. 6. Discharge profiles in the 1st cycle and the 50th cycle with $T_{\text{air}} = 55^\circ\text{C}$ and $V_{\text{cell}} = [3.5, 4.3]$ V.

Appendix A

The P2D model is summarized as follows.

In the cathode:

The governing equation for the charge balance in the solid phase in the cathode:

$$\frac{\partial i_1}{\partial x} = -a_p F j_p \quad (39)$$

where a_p is the specific area of the active material in the cathode, F is Faraday's constant, j_p is the pore wall flux and the solid phase current density, i_1 , is defined by:

$$i_1 = -\sigma_{\text{eff},p} \frac{\partial \phi_1}{\partial x} \quad (40)$$

where $\sigma_{\text{eff},p}$ is the effective electronic conductivity of the cathode, and ϕ_1 is the solid phase potential. The effective electronic conductivity for the electrodes is determined by the following equation:

$$\sigma_{\text{eff},i} = \sigma_i \varepsilon_{v,i}^{\text{brugg}_i}, \quad i = p, n \quad (41)$$

where σ_i denotes the electronic conductivity of the dense material in electrode i and brugg_i is the Bruggeman number of electrode i .

At the cathode/current collector interface ($x = L_p + L_s + L_n$), the entire current density is carried by the solid phase. That is:

$$i_1|_{x=L_p+L_s+L_n} = I_{\text{app}} \quad (42)$$

where I_{app} is the applied current density (the current which is divided by the projected electrode area), I_{app} is positive when charging the cell and negative when discharging the cell.

At the separator/cathode interface, no current is carried by the solid phase:

$$i_1|_{x=L_n+L_s} = 0 \quad (43)$$

The charge balance in the electrolyte is given by:

$$\frac{\partial i_2}{\partial x} = a_p F j_p \quad (44)$$

where the current density in the electrolyte filled in the cathode, i_2 , is defined by:

$$i_2 = -\kappa_{\text{eff},p} \frac{\partial \phi_2}{\partial x} + \frac{2\kappa_{\text{eff},p}RT}{F} (1 - t_+^0) \frac{\partial \ln c}{\partial x} \quad (45)$$

where $\kappa_{\text{eff},p}$ is the effective ionic conductivity of the electrolyte in the cathode, ϕ_2 is the electrolyte potential, R is the universal gas constant, T is the temperature and t_+^0 is the transference number and c is the concentration of the binary electrolyte.

At $x = L_p + L_s + L_n$, there is no current in the electrolyte passing through the cathode/current collect interface:

$$i_2|_{x=L_p+L_s+L_n} = 0 \quad (46)$$

At $x = L_n + L_s$, the current density in the electrolyte at the separator/cathode interface is continuous:

$$i_2|_{x=(L_n+L_s)^-} = i_2|_{x=(L_n+L_s)^+} \quad (47)$$

The solution phase concentration in the cathode is given by the material balance on the electrolyte phase:

$$\frac{\partial (\varepsilon_p c)}{\partial t} = \frac{\partial}{\partial x} \left(D_{\text{eff},p} \frac{\partial c}{\partial x} \right) + (1 - t_+^0) a_p j_p \quad (48)$$

where ε_p is the porosity of the cathode, $D_{\text{eff},p}$ is the effective diffusion coefficient of Li^+ in the binary electrolyte in the cathode. The initial concentration of the electrolyte is set to a known constant, c_0 :

$$c(t = 0) = c_0 \quad (49)$$

The flux of Li^+ in the electrolyte at the cathode/current collector interface is zero:

$$-D_{\text{eff},p} \frac{\partial c}{\partial x} \Big|_{x=L_p+L_s+L_n} = 0 \quad (50)$$

The flux is continuous at the separator/cathode interface:

$$-D_{\text{eff},s} \frac{\partial c}{\partial x} \Big|_{x=(L_n+L_s)^-} = -D_{\text{eff},p} \frac{\partial c}{\partial x} \Big|_{x=(L_n+L_s)^+} \quad (51)$$

In the separator:

The solution phase concentration in the separator is governed by:

$$\frac{\partial (\varepsilon_s c)}{\partial t} = \frac{\partial}{\partial x} \left(D_{\text{eff},s} \frac{\partial c}{\partial x} \right) \quad (52)$$

where ε_s is the porosity of the separator and $D_{\text{eff},s}$ is the diffusion coefficient of Li^+ in the electrolyte in the separator. The initial concentration of the electrolyte is set to a known constant, c_0 :

$$c(t = 0) = c_0 \quad (53)$$

The fluxes of Li^+ in the electrolyte at the anode/separator and separator/cathode interfaces are continuous:

$$-D_{\text{eff},n} \frac{\partial c}{\partial x} \Big|_{x=L_n^-} = -D_{\text{eff},s} \frac{\partial c}{\partial x} \Big|_{x=L_n^+} \quad (54)$$

$$-D_{\text{eff},s} \frac{\partial c}{\partial x} \Big|_{x=(L_n+L_s)^-} = -D_{\text{eff},p} \frac{\partial c}{\partial x} \Big|_{x=(L_n+L_s)^+} \quad (55)$$

where $D_{\text{eff},n}$ is the diffusion coefficient of Li^+ in the electrolyte in the anode. It should note that the concentration of Li^+ at the interfaces is also continuous, in another words, there is no concentration jump at the interfaces.

Because there is no active solid phase in the separator, all currents are carried by the electrolyte, that is:

$$\frac{\partial i_2}{\partial x} = 0 \quad (56)$$

where the current density in the electrolyte in the separator is given by:

$$i_2 = -\kappa_{\text{eff},s} \frac{\partial \phi_2}{\partial x} + \frac{2\kappa_{\text{eff},s}RT}{F} (1 - t_+^0) \frac{\partial \ln c}{\partial x} \quad (57)$$

where $\kappa_{\text{eff},s}$ is the effective ionic conductivity of the electrolyte in the separator.

The current densities at the anode/separator and separator/cathode interfaces are continuous:

$$i_2|_{x=L_n^-} = i_2|_{x=L_n^+} \quad (58)$$

$$i_2|_{x=(L_n+L_s)^-} = i_2|_{x=(L_n+L_s)^+} \quad (59)$$

In the anode:

The charge balance in the solid phase in the anode is given by:

$$\frac{\partial i_1}{\partial x} = -a_n F j_n \quad (60)$$

where a_n is the specific of the active material in the anode, j_n is the pore wall flux in the anode and the current density in the solid phase in the anode, i_1 , is defined by:

$$i_1 = -\sigma_{\text{eff},n} \frac{\partial \phi_1}{\partial x} \quad (61)$$

where $\sigma_{\text{eff},n}$ is the electronic conductivity of the solid phase in the anode. The boundary conditions for ϕ_1 are:

$$i_1|_{x=0} = I_{\text{app}} \text{ and } i_1|_{x=L_n} = 0 \quad (62)$$

The potential in the solution phase in the anode is given by:

$$\frac{\partial i_2}{\partial x} = a_n F j_n \quad (63)$$

where the current density in the electrolyte in the anode, i_2 , is defined by:

$$i_2 = -\kappa_{\text{eff},n} \frac{\partial \phi_2}{\partial x} + \frac{2\kappa_{\text{eff},n} RT}{F} (1 - t_+^0) \frac{\partial \ln c}{\partial x} \quad (64)$$

where $\kappa_{\text{eff},n}$ is the effective ionic conductivity of the electrolyte in the anode.

The boundary conditions for ϕ_2 in the anode are:

$$\phi_2|_{x=0} = 0 \text{ and } i_2|_{x=L_n^-} = i_2|_{x=L_n^+} \quad (65)$$

where the solution phase potential at $x = 0$ is set as the reference potential.

The material balance in the electrolyte in the anode is given by:

$$\frac{\partial (\varepsilon_n c)}{\partial t} = \frac{\partial}{\partial x} \left(D_{\text{eff},n} \frac{\partial c}{\partial x} \right) + (1 - t_+^0) a_n j_n \quad (66)$$

where ε_n is the porosity of the anode, $D_{\text{eff},n}$ is the diffusion coefficient of Li^+ in the binary electrolyte in the anode. The initial concentration of the electrolyte is set to a known constant, c_0 :

$$c(t = 0) = c_0 \quad (67)$$

The flux of Li^+ at the current collector/anode interface is zero:

$$-D_{\text{eff},n} \frac{\partial c}{\partial x}|_{x=0} = 0 \quad (68)$$

The flux at the anode/separator interface is continuous as shown in Eq. (54).

The concentration of Li^+ in the particles in the anode is given by the Fick's law in the spherical coordinates:

$$\frac{\partial c_{s,n}}{\partial t} = \frac{1}{r^2} \frac{\partial}{\partial r} \left(r^2 D_{s,n} \frac{\partial c_{s,n}}{\partial r} \right) \quad (69)$$

where $D_{s,n}$ is the diffusion coefficient of Li^+ in the particles in the anode. The initial condition is:

$$c_{s,n}(t = 0) = c_{s,n,0} \quad (70)$$

where $c_{s,n,0}$ is the initial concentration of Li^+ in the particles in the anode. And the boundary conditions for the anode particles are:

$$-D_{s,n} \frac{\partial c_{s,n}}{\partial r}|_{r=0} = 0 \quad (71)$$

and

$$-D_{s,n} \frac{\partial c_{s,n}}{\partial r}|_{r=R_n} = j_n \quad (72)$$

where R_n is the radius of the particles in the anode.

Appendix B

Expressions

The pore wall flux at the surface of the particles in electrode i is related to the potentials in the solid and solution phases through the Butler–Volmer type kinetics equation:

$$j_i = k_i c_{s,i,\text{surf}}^{0.5} \left(c_{s,i,\text{max}} - c_{s,i,\text{surf}} \right)^{0.5} c_i^{0.5} \left(\exp \left(\frac{\alpha_{a,p} F}{R T_i} \eta_i \right) - \exp \left(-\frac{\alpha_{c,p} F}{R T_i} \eta_i \right) \right) \quad (73)$$

where k_i is the reaction rate constant in electrode i , $c_{s,i,\text{surf}}$ is the surface concentration of Li^+ in the particles in electrode i , $c_{s,i,\text{max}}$ is the maximum concentration of Li^+ in the particles in electrode i , η_i is the overpotential on electrode i . The overpotentials on the cathode and the anode are defined as follows:

$$\eta_p = \phi_{1,p} - \phi_{2,p} - U_p - R_{\text{film}} F j_p \quad (74)$$

$$\eta_n = \phi_{1,n} - \phi_{2,n} - U_n \quad (75)$$

The open circuit potentials in the electrodes are functions of temperature and states of charge (SOC) of the electrodes as follows:

$$U_i = U_{i,\text{ref}} + (T_i - T_{\text{ref}}) \left[\frac{\partial U}{\partial T} \right]_i \quad (76)$$

where $U_{i,\text{ref}}$ is the open circuit potential as a function of state of charge (SOC) measured at the reference temperature, T_{ref} .

The open circuit potentials at $T_{\text{ref}} = 25$ °C for the LiMn_2O_4 cathode and for the carbon anode as functions of state of charge are given by [20]:

$$\begin{aligned} U_{p,\text{ref}} = & 4.19829 + 0.0565661 \tan h(-14.5546 \theta_p + 8.60942) \\ & - 0.0275479 \left(\frac{1}{(0.998432 - \theta_p)^{0.492465}} - 1.90111 \right) \\ & - 0.157123 \exp(-0.04738 \theta_p^8) \\ & + 0.810239 \exp(-40(\theta_p - 0.133875)) \end{aligned} \quad (77)$$

and

$$U_{n,\text{ref}} = -0.16 + 1.32 \exp(-3\theta_n) + 10 \exp(-2000\theta_n) \quad (78)$$

where the SOC is defined by:

$$\theta_i = \frac{c_{s,i,\text{surf}}}{c_{s,i,\text{max}}}, \quad i = p, n \quad (79)$$

The $[\partial U/\partial T]_p$ data as a function of SOC for LiMn_2O_4 reported by Thomas et al. [25] was refitted to an empirical equation presented by Srinivasan and Wang [26] as follows:

$$\begin{aligned} \left[\frac{\partial U}{\partial T} \right]_p = & a_1 \exp(a_2 \theta_p) + a_3 \sin(a_4 \theta_p) + a_5 \sin(a_6 \theta_p + a_7) \\ & + a_8 \sin(a_9 \theta_p + a_{10}) + b_0 + b_1 \theta_p + b_2 \theta_p^2 + b_3 \theta_p^3 \\ & + b_4 \left(\exp \left(-\frac{\theta_p + b_5}{b_6} \right) \right)^2 \end{aligned} \quad (80)$$

$$k_i = 10^{-4} \times c_i \left(\frac{-10.5 + 0.668 \times 10^{-3} c_i + 0.494 \times 10^{-6} c_i^2 + 0.074 T_i}{-1.78 \times 10^{-5} c_i T_i - 8.86 \times 10^{-10} c_i^2 T_i - 6.96 \times 10^{-5} T_i^2 + 2.80 \times 10^{-8} c_i T_i^2} \right)^2 \quad (85)$$

where: $a_1 = -272.45547143156853$, $a_2 = -8.4660463364774969$, $a_3 = 3.9548818181675394$, $a_4 = -6.3644778205164450$, $a_5 = -0.11494477221293507$, $a_6 = -26.341590055374475$, $a_7 = 28.202482124134448$, $a_8 = -0.0045805692645594738$, $a_9 = 114.74983936455860$, $a_{10} = -72.387775508734848$, $b_0 = 53.722802544438963$, $b_1 = -164.19140744090566$, $b_2 = 136.83084104679463$, $b_3 = -26.071652680281360$, $b_4 = 0.74302471734078734$, $b_5 = -0.53278657307359123$, $b_6 = 0.18367552820218680$, and the unit for $[\partial U/\partial T]_p$ is mV K⁻¹.

The $[\partial U/\partial T]_n$ as a function of SOC for a carbon-based anode (meso carbon micro beads, MCMB) was measured at USC and was fitted to the following empirical equation:

$$\left[\frac{\partial U}{\partial T} \right]_n = \frac{a_0 + a_1 \theta_n + a_2 \theta_n^2 + a_3 \theta_n^3 + a_4 \theta_n^4 + a_5 \theta_n^5 + a_6 \theta_n^6 + a_7 \theta_n^7 + a_8 \theta_n^8}{1 + b_1 \theta_n + b_2 \theta_n^2 + b_3 \theta_n^3 + b_4 \theta_n^4 + b_5 \theta_n^5 + b_6 \theta_n^6 + b_7 \theta_n^7 + b_8 \theta_n^8} \quad (81)$$

where: $a_0 = 0.005269056$, $a_1 = 3.299265709000005$, $a_2 = -91.79325798000001$, $a_3 = 1004.911008$, $a_4 = -5812.278127$, $a_5 = 19.329.7549$, $a_6 = -37.147.8947$, $a_7 = 38.379.18127$, $a_8 = -16.515.05308$, $b_1 = -48.09287227$, $b_2 = 1017.234804$, $b_3 = -10.481.80419$, $b_4 = 59.431.30001$, $b_5 = -195.881.6488$, $b_6 = 374.577.3152$, $b_7 = -385.821.1607$, $b_8 = 165.705.8597$, and the unit for $[\partial U/\partial T]_n$ is mV K⁻¹.

The temperature dependent reaction rate constants for the electrodes are determined by:

$$k_i = k_{i,\text{ref}} \exp \left(\frac{E_{ak,i}}{R} \left(\frac{1}{T_{\text{ref}}} - \frac{1}{T} \right) \right) \quad (82)$$

where $k_{i,\text{ref}}$ is the reaction rate constant for electrode i at the reference temperature, T_{ref} , $E_{ak,i}$ is the activation energy related to the reaction rate constant for electrode i .

The temperature dependent diffusion coefficient of Li⁺ in the solid phase is given by:

$$D_{s,i} = D_{s,i,\text{ref}} \exp \left(\frac{E_{ad,i}}{R} \left(\frac{1}{T_{\text{ref}}} - \frac{1}{T} \right) \right) \quad (83)$$

where $D_{s,i,\text{ref}}$ is the diffusion coefficient of Li⁺ in the solid particle in electrode i , $E_{ad,i}$ is the activation energy related to the diffusion coefficient of Li⁺ in the solid phase in electrode i .

The specific area of the active material in electrode i is related to the volume fraction of the active materials in electrode i as follows:

$$a_p = \frac{3}{R_{a,p}} \varepsilon_{v,p} \quad \text{and} \quad a_n = \frac{3}{R_n} \varepsilon_{v,n} \quad (84)$$

The concentration and temperature dependent ionic conductivity and the diffusion coefficient in the binary electrolyte are given by [27]:

$$D_i = 10^{-4} \times 10^{-4.43 - \frac{54}{T_i - 229 - 5.0 \times 10^{-3} c_i} - 0.22 \times 10^{-3} c_i} \quad (86)$$

The effective ionic conductivity and diffusion coefficient in the binary electrolyte are determined by the following equations, respectively:

$$\kappa_{\text{eff},i} = \kappa_i \varepsilon_i^{\text{bruggi}}, \quad i = p, s, n \quad (87)$$

$$D_{\text{eff},i} = D_i \varepsilon_i^{\text{bruggi}}, \quad i = p, s, n \quad (88)$$

The cell voltage is determined as the difference in the solid phase potentials between the two ends of the cell:

$$V_{\text{cell}} = \phi_1|_{x=L_n+L_s+L_p} - \phi_1|_{x=0} \quad (89)$$

List of symbols

a_i	specific surface area of electrode i ($i = p, n$), $\text{m}^2 \text{m}^{-3}$
bruggi	Bruggeman coefficient of region i ($i = p, s, n$)
c	electrolyte concentration, mol m^{-3}
c_0	initial electrolyte concentration, mol m^{-3}
$c_{s,i}$	concentration of lithium ions in the intercalation particle of electrode i ($i = p, n$), mol m^{-3}
$c_{s,i,0}$	initial concentration of lithium ions in the intercalation particle of electrode i ($i = p, n$), mol m^{-3}
$c_{s,i,\text{max}}$	maximum concentration of lithium ions in the intercalation particle of electrode i ($i = p, n$), mol m^{-3}
D	electrolyte diffusion coefficient, $\text{m}^2 \text{s}^{-1}$
$D_{s,i}$	lithium ion diffusion coefficient in the intercalation particle of electrode i ($i = p, n$), $\text{m}^2 \text{s}^{-1}$
F	Faraday's constant, $96,487 \text{ C equiv}^{-1}$
h_{coef}	heat transfer coefficient, $\text{W m}^{-2} \text{K}^{-1}$
I_{app}	applied current density, A m^{-2}
i_1	solid phase current density, A m^{-2}
i_2	solution phase current density, A m^{-2}

j_i	wall flux of Li^+ on the intercalation particle of electrode i ($i = p, n$), $\text{mol m}^{-2} \text{s}^{-1}$
k_i	intercalation/deintercalation reaction rate constant of electrode i ($i = p, n$), $\text{mol}^{0.5} \text{m}^{2.5} \text{s}^{-1}$
L_i	thickness of region i ($i = p, s, n$), m
n	negative electrode
p	positive electrode
r	radial coordinate, m
R	universal gas constant, $\text{J mol}^{-1} \text{K}^{-1}$
R_{ap}	radius of the active spinel, m
R_{film}	film resistance at the cathode, Ωm^2
R_i	initial radius of the intercalation particle of electrode i ($i = p, n$), m
R_{sp}	radius of the solid particle in the cathode, m
t_+^0	Li^+ transference number in the electrolyte
T	absolute temperature, K
U_i	open circuit potential of electrode i ($i = p, n$), V
x	spatial coordinate, m
ε_i	porosity of region i ($i = p, s, n$)
$\varepsilon_{f,i}$	volume fraction of fillers of electrode i ($i = p, n$)
$\varepsilon_{iv,p}$	volume fraction of the inactive material in cathode
θ_i	dimensionless concentration of lithium ions in the intercalation particle of electrode i ($\theta_i = c_{\text{s},i,\text{surf}}/c_{\text{s},i,\text{max}}$)
κ	ionic conductivity of the electrolyte, S m^{-1}
$\kappa_{\text{eff},i}$	effective ionic conductivity of the electrolyte in region i ($i = p, s, n$), S m^{-1}
σ_i	electronic conductivity of the solid phase of electrode i ($i = p, n$), S m^{-1}
$\sigma_{\text{eff},i}$	effective electronic conductivity of the solid phase of electrode i ($i = p, n$), S m^{-1}
ϕ_1	solid phase potential, V
ϕ_2	solution phase potential, V

References

- [1] M. Wohlfahrt-Mehrens, C. Vogler, J. Garche, J. Power Sources 127 (2004) 58–64.
- [2] W. Choi, A. Manthiram, J. Electrochem. Soc. 153 (2006) A1760–A1764.
- [3] P. Arora, R.E. White, M. Doyle, J. Electrochem. Soc. 145 (1998) 3647–3667.
- [4] Y.Y. Xia, Y.H. Zhou, M. Yoshio, J. Electrochem. Soc. 144 (1997) 2593–2600.
- [5] D.H. Jang, Y.J. Shin, S.M. Oh, J. Electrochem. Soc. 143 (1996) 2204–2211.
- [6] L.F. Wang, C.C. Ou, K.A. Striebel, J.J.S. Chen, J. Electrochem. Soc. 150 (2003) A905–A911.
- [7] T. Aoshima, K. Okahara, C. Kiyohara, K. Shizuka, J. Power Sources 97 (2001) 377–380.
- [8] T. Inoue, M. Sano, J. Electrochem. Soc. 145 (1998) 3704–3707.
- [9] D. Aurbach, M.D. Levi, K. Gamolski, B. Markovsky, G. Salitra, E. Levi, U. Heider, L. Heider, R. Oesten, J. Power Sources 81 (1999) 472–479.
- [10] D. Kim, S. Park, O.B. Chae, J.H. Ryu, Y.U. Kim, R.Z. Yin, S.M. Oh, J. Electrochem. Soc. 159 (2012) A193–A197.
- [11] T. Eriksson, A.M. Andersson, A.G. Bishop, C. Gejke, T. Gustafsson, J.O. Thomas, J. Electrochem. Soc. 149 (2002) A69–A78.
- [12] D. Aurbach, K. Gamolsky, B. Markovsky, G. Salitra, Y. Gofer, U. Heider, R. Oesten, M. Schmidt, J. Electrochem. Soc. 147 (2000) 1322–1331.
- [13] J. Park, J.H. Seo, G. Plett, W. Lu, A.M. Sastry, Electrochim. Solid-State Lett. 14 (2011) A14–A18.
- [14] C.H. Lu, S.W. Lin, J. Mater. Res. 17 (2002) 1476–1481.
- [15] M. Doyle, T.F. Fuller, J. Newman, J. Electrochem. Soc. 140 (1993) 1526–1533.
- [16] V. Srinivasan, J. Newman, J. Electrochem. Soc. 151 (2004) A1517–A1529.
- [17] Q. Zhang, R.E. White, J. Electrochem. Soc. 154 (2007) A587–A596.
- [18] B.C. Han, A. Van der Ven, D. Morgan, G. Ceder, Electrochim. Acta 49 (2004) 4691–4699.
- [19] L. Cai, R.E. White, J. Electrochem. Soc. 157 (2010) A1188–A1195.
- [20] M. Doyle, J. Newman, A.S. Gozdz, C.N. Schmutz, J.M. Tarascon, J. Electrochem. Soc. 143 (1996) 1890–1903.
- [21] SUNDIALS, online: <https://computation.llnl.gov/casc/sundials/main.html>, (accessed 20.03.12).
- [22] COMSOL Multiphysics®, online: <http://www.comsol.com/>, (accessed 20.03.12).
- [23] R.J. Gummow, A. de Kock, M.M. Thacheray, Solid State Ionics 69 (1994) 59–67.
- [24] A. Du Pasquier, A. Blyr, P. Courjal, D. Larcher, G. Amatucci, B. Gerand, J.-M. Tarascon, J. Electrochem. Soc. 146 (1999) 428–436.
- [25] K.E. Thomas, C. Bogatu, J. Newman, J. Electrochem. Soc. 148 (2001) A570–A575.
- [26] V. Srinivasan, C.Y. Wang, J. Electrochem. Soc. 150 (2003) A98–A106.
- [27] L.O. Valoen, J.N. Reimers, J. Electrochem. Soc. 152 (2005) A882–A891.